J Oceanogr (2016) 72:697–705
DOI 10.1007/s10872-016-0363-3

ORIGINAL ARTICLE

Contribution of sea-surface wind curl to the maintenance of the SST gradient along the upstream Kuroshio Extension in early summer

Naoki Sato[1,2] · Masami Nonaka[2] · Yoshikazu Sasai[2] · Hideharu Sasaki[2] · Youichi Tanimoto[2,3] · Ryuichi Shirooka[2]

Received: 19 December 2014 / Revised: 1 March 2016 / Accepted: 3 March 2016 / Published online: 21 March 2016

Abstract The seasonal cycle of the meridional sea-surface temperature (SST) gradient in the upstream Kuroshio Extension (KE) region was examined using satellite observation data and model simulations. In general, the meridional SST gradient is small in summer. However, in early summer (June and July), the SST front is sustained or intensified on the northern side of the KE near the coast of eastern Japan. This observed seasonal cycle was successfully simulated in the North Pacific Ocean model for the Earth Simulator (NP-OFES). Analysis of the forecast data revealed that the vertical profiles of temperature and salinity are shifted upward along the KE in early summer. As a result, the permanent thermocline depth is shallowest during summer, causing a relatively small SST tendency. In addition, significant cyclonic vorticity in the lower atmosphere related to the southwesterly sea-surface wind was found to the south of the KE, associated with the Baiu frontal zone (BFZ). It was inferred that the positive vorticity causes Ekman upwelling over the KE region, resulting in suppressed SST warming on the northern side of the KE. These results suggest that the BFZ contributes to maintaining or strengthening the SST front.

Keywords Kuroshio Extension · Baiu · SST front · Ekman upwelling · OGCM

✉ Naoki Sato
snaoki@u-gakugei.ac.jp

[1] Tokyo Gakugei University, Koganei 184-8501, Japan

[2] Japan Agency for Marine-Earth Science and Technology, Yokosuka 237-0061, Japan

[3] Faculty of Environmental Earth Science, Graduate School of Environmental Science, Hokkaido University, Sapporo 060-0808, Japan

1 Introduction

The Kuroshio is the western boundary current of the North Pacific subtropical gyre. It flows northeastward along the continental slope in the East China Sea and then eastward along the southern coast of Japan. After reaching the eastern tip of Japan, it forms an eastward current called the Kuroshio Extension (KE). The Kuroshio is one of the most predominant western boundary currents, along with the Gulf Stream (GS). Previous studies investigated the air-sea interaction over the KE and the GS (Kwon et al. 2010), especially focusing on the ocean's role in decadal time scale variability (Nonaka et al. 2006, 2008; Taguchi et al. 2007, 2010) and its predictability (Qiu et al. 2014; Nonaka et al. 2012). In general, the warm KE releases abundant heat and moisture into the atmosphere, especially in the cold seasons, implying a significant impact of the KE on the atmospheric circulation (Taguchi et al. 2009; Tanimoto et al. 2011). Furthermore, the frontal gradient in the sea-surface temperature (SST) associated with a warm western boundary current can affect atmospheric disturbances aloft (e.g., Minobe et al. 2008; Nakamura et al. 2012). These studies investigated the effects of SST fronts on the atmosphere. Most of these previous studies on the role of fronts in the mid-latitude ocean focused on the cold seasons, when a large heat flux is released into the atmosphere.

Inversely, the surface wind over the SST front may affect the thermodynamics of the ocean. For example, Xue et al. (1995) demonstrated that Ekman transport plays a role in modifying the Gulf Stream. In addition, Alexander and Scott (2008) also revealed the role of Ekman transport across the SST front in the interannual variability of the mid-latitude ocean. Furthermore, the role of the surface wind on smaller spatial scales has been also examined.

For example, in the subtropics, Xie et al. (2003) demonstrated that the SST distribution is modulated by Ekman upwelling associated with a strong summertime monsoonal wind. Sato et al. (2006) found that mechanical mixing due to strong surface wind also affects the SST in the subtropical ocean. These effects of the surface wind are predominant where the mixed layer depth is shallow. In general, the mixed layer becomes shallow in summer in the mid-latitude ocean. However, the influence of sea-surface wind on the SST distribution in the summertime KE region in a small horizontal scale has not been examined in detail.

In early summer (June and July), the Baiu frontal zone (BFZ) is situated over the Kuroshio/KE regions. A rainy season Baiu is brought by the BFZ in the mainland of Japan. The BFZ is regarded as the western part of the Pacific Polar frontal zone generated along the boundary between the maritime tropical airmass and the maritime polar airmass (Yoshimura 1967; Akiyama 1973). It is also recognized as a rain belt along the southern coast of the mainland of Japan during June and July. It gradually moves northward during Baiu, in association with the western extension of the Pacific anticyclone. Across the BFZ, the difference in low-level equivalent potential temperature is large (Akiyama 1973). On the southern side of the BFZ, hot and moist low-level air is favored by active cumulus convection (Ninomiya 2000). This hot and moist airmass is formed over high-SST regions. However, low SST brings low-level stratiform clouds on the northern side of the BFZ, which are sometimes associated with the cold northeasterly wind called Yamase (Ninomiya and Mizuno 1985). From these observations, it is inferred that the SST difference across the front substantially affects the BFZ through the two different airmasses. In addition, a strong low-level westerly or southwesterly wind is often observed during Baiu. According to Akiyama (1973), this westerly is mainly caused by vertical mixing related to active cumulus convection. Considering some recent results such as those of Xie et al. (2003) and Sato et al. (2006), the strong westerly wind may influence the oceanic condition along the KE.

In order to reveal the oceanic response to the atmosphere, in situ measurement data taken in the ocean are required, since satellite measurements cannot directly capture dynamic and thermodynamic fields in the subsurface layer of the ocean. Recently, for example, Argo profiling floats automatically obtained vertical profiles for sea-water temperature and salinity over all of the oceans at 10-day intervals (Argo Science Team 2001). However, a small number of profiles are obtained by the floats in the Kuroshio/KE regions, since a float cannot stay in these regions for a long period because of the high current velocity. The number of ship measurements is also limited. Therefore, the oceanic response to the strong westerly or southwesterly wind in early summer has not yet been investigated in detail.

The present study examines the seasonal march of the ocean along the KE during Baiu using both satellite observation and model data. Since the BFZ accompanies mesoscale convection systems over Japan, we focus on the air-sea coupling in a relatively small region near Japan. The climatological seasonal march of the SST over the KE region is first examined by using satellite observation data. The observations are then compared with a high-resolution ocean general circulation model (OGCM). The data and results are provided in Sects. 2 and 3, respectively. We discuss the results and give our conclusions in Sect. 4.

2 Data

2.1 Observations

Satellite observational absolute dynamic topography (ADT) data, distributed by the data archiving center Archiving, Validation and Interpretation of Satellite Oceanographic data (AVISO) (CNES 2014), were first used to infer near-surface currents around the KE region. The data set was a merged satellite observation that was taken from Haiyang-2A (HY-2A), SARAL/AltiKa, CryoSat-2, Jason-1, Jason-2, TOPEX/Poseidon, Environmental Satellite (Envisat), Geosat Follow-On (GFO), European Remote Sensing-1/2 (ERS-1/2) and Geosat data. We used the delayed time product. The horizontal resolution is $0.25° \times 0.25°$. The climatological means for June and July were obtained by averaging daily data from 2001 to 2010.

Tropical Rainfall Measuring Mission (TRMM) Microwave Imager (TMI) SST data (Wentz et al. 2000) were then used to examine the seasonal changes in SST averaged from 2001 to 2010 around the KE region. The TMI SST data were provided by remote sensing systems (RSS). This SST data set has a resolution of $0.25° \times 0.25°$. For simplicity, the daily data sets were edited first. Missing values caused by the lack of a path width were replaced with temporally interpolated values at each grid point. Linear interpolation was applied here. In most cases, at least one observed value is available during an arbitrary 3-day period at each grid. No spatial interpolation was carried out in order to capture spatially fine structures of the SST front. We focused on the difference between the SST distributions in June and July. According to Qiu et al. (2014), the KE modulates between a stable and unstable state. To examine whether the seasonal march depends on the modulation, the SST difference between June and July only for unstable years (2001, 2006, 2007, 2008, and 2009) was also analyzed. After that, we analyzed a latitude section of the seasonal cycle of SST averaged from 140°E to 144°E.

For comparison, another latitude section from 144°E to 148°E was also examined.

In general, the surface wind can affect the SST through air-sea coupling. Thus, the strong westerly or southwesterly wind associated with the BFZ may play a role in modulating SST in the Kuroshio/KE regions during early summer. Therefore, Quick Scatterometer (QuikScat) sea-surface wind data (Wentz and Smith 1999) were then examined in June and July corresponding to the seasonal march of the SST. The QuikScat data were provided by RSS. These sea-surface wind data also have a resolution of 0.25° × 0.25°. The surface wind was averaged from 2001 to 2009, since QuikScat data have not been available since November of 2009. In addition, the relative vorticity was calculated for the surface wind.

The relationship between the surface wind and the rain belt associated with the BFZ was then confirmed using the Global Satellite Mapping of Precipitation (GSMaP) data (Aonashi and Liu 2000). In the present study, the daily product in the GSMaP_MVK Version 5 was used. The horizontal resolution was 0.1° × 0.1°.

2.2 Model simulation

The seasonal march in the ocean was then examined, focusing on the oceanic response to the surface wind. In order to investigate the detailed seasonal variability in the ocean with fine resolution, hindcast data simulated by an ocean model were used. In the present study, we utilized the Modular Ocean Model 3 (MOM3) OGCM (Pacanowski and Griffies 2000) with substantial modifications for optimal performance on the vector-parallel hardware system of Japan's Earth Simulator. This North Pacific Ocean model for the Earth Simulator (NP-OFES) (Sasaki and Klein 2012) with sea ice (Komori et al. 2005) covers nearly the whole North Pacific domain (20°S–68°N, 100°E–70°W). A long-time integration with a relatively high resolution was conducted by running the model within the North Pacific domain instead of the global domain. In Sasaki and Klein (2012), the NP-OFES successfully simulated the dynamic field in the North Pacific including relatively small disturbances in the KE region. Although the model simulation was performed in the North Pacific domain, it appears that the influence of the lateral boundary was not large since the KE region is not near the boundary. In the present study, we used the 0.1° horizontal resolution integration of NP-OFES introduced by Sasaki and Klein (2012). It has 54 vertical levels with 5-m resolution just below the surface, and the maximum depth is 6065 m.

The NP-OFES was forced by surface-wind stress, heat, and freshwater fluxes derived from the Japanese 25-year Reanalysis (JRA-25) data (Onogi et al. 2007), which has a horizontal resolution of 1.25° × 1.25°. On the other hand, the ocean model has a horizontal resolution of 0.1°. Thus, the JRA-25 data including wind stress data are much coarser than the model grid. However, since the climatological Baiu is basically a synoptic or meso-α-scale phenomenon (Ninomiya 2000), the sea-surface wind data obtained from JRA-25 seem to successfully represent the fundamental properties of the low-level jet. Therefore, the NP-OFES probably estimates the effect of surface wind on the ocean well even using JRA-25 data in which small-scale disturbances are unresolved. As wind stress data, satellite-borne microwave scatterometer observations are assimilated in the JRA-25. Satellite observation implicitly includes the dependency of wind stress on ocean current. Thus, it is supposed that the difference of wind stress caused by the ocean current is partly reflected in the boundary condition obtained from the JRA-25. However, the NP-OFES does not explicitly estimate the dependency of wind stress on the variation of the simulated ocean current.

First, we conducted a 15-year integration with long-term (1979–2004) mean 6-hourly forcing (climatological integration). A hindcast integration with 6-hourly atmospheric fields taken from the JRA-25 was then conducted covering 1979–2012. Corresponding to the observation data, we analyzed data from 2001 to 2010. Some previous studies reproduced the ocean dynamics well by using OGCM for a quasi-global domain (Masumoto et al. 2004; Sasaki et al. 2008). In recent years, the climatological features as well as the interannual-to-decadal variability in the western North Pacific were investigated in detail using OGCM (Nonaka et al. 2006, 2008, 2012; Taguchi et al. 2007, 2010).

3 Results

3.1 Observations

According to the ADT data, the meridional ADT gradient is large along a latitude line of 35°N corresponding to the Kuroshio and KE in June (the top panel of Fig. 1). In these regions, a strong eastward current exists. A similar result is also obtained in July, although the meridional ADT difference across the Kuroshio/KE becomes somewhat large and moves slightly southward from June to July. Figure 2 indicates the averaged SSTs for June and July 2001–2010. A large meridional SST gradient is observed north of 35°N. The gradient is especially large between 35°N and 36°N near the KE. To the west of 145°E, the SST gradient has two peaks (around 35.5°N and 38.5°N). Moreover, Fig. 3 indicates that the increase of SST from June to July is relatively small on the northern side of the SST front in the KE region near Japan, while the SST increase is larger on the southern side. This means that the meridional gradient of

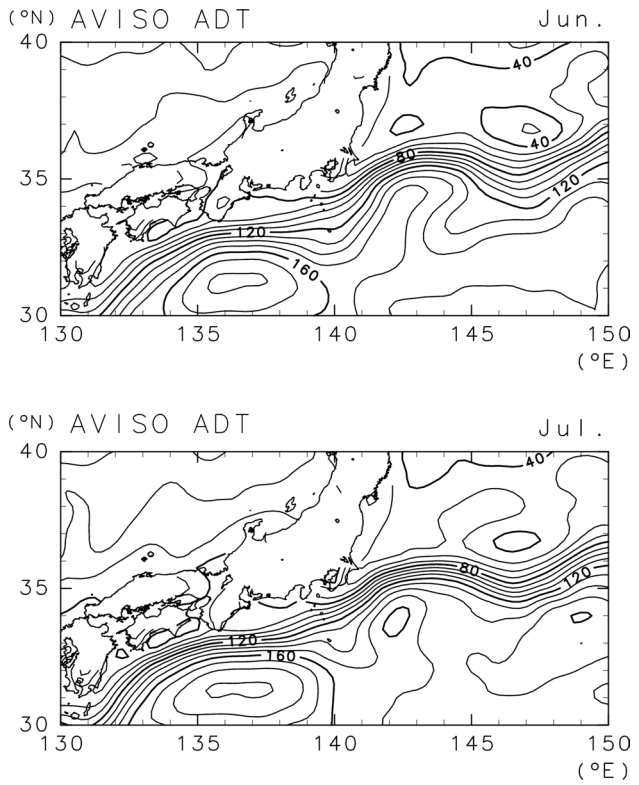

Fig. 1 ADT averaged for (*top*) June and (*bottom*) July from 2001 to 2010. The contour interval is 10 cm

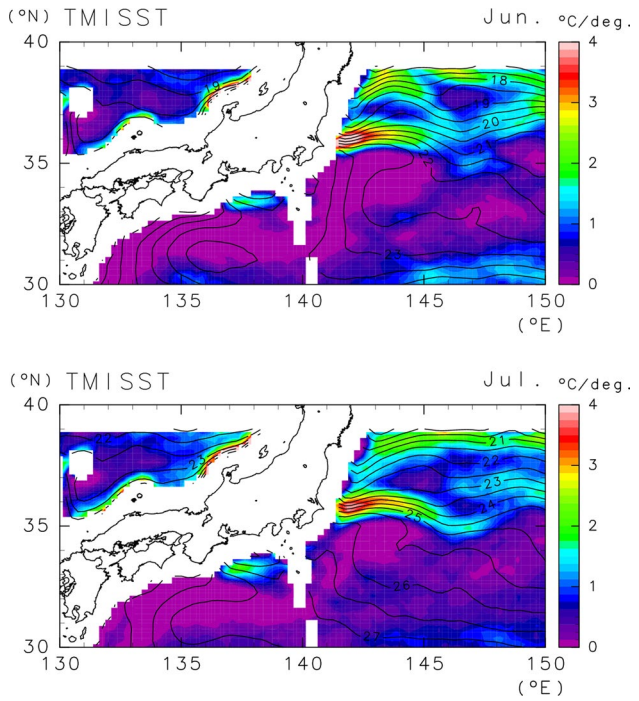

Fig. 2 SST (contours) and its meridional gradient (tones) averaged for (*top*) June and (*bottom*) July from 2001 to 2010. The contour interval is 0.5 °C

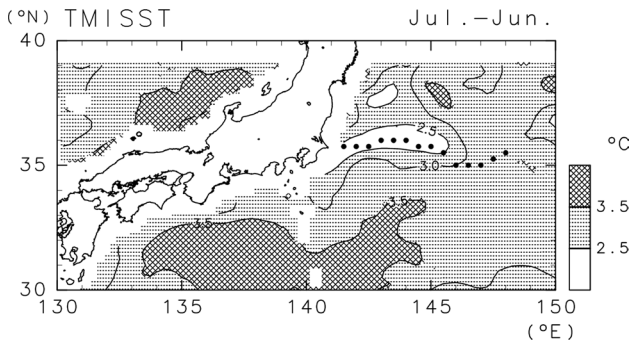

Fig. 3 Difference in SSTs between June and July averaged from 2001 to 2010. The contour interval is 0.5 °C. Values exceeding 2.5 °C (3.5 °C) are *shaded* (*hatched*). *Dots* indicate the maximum of meridional SST gradient in July

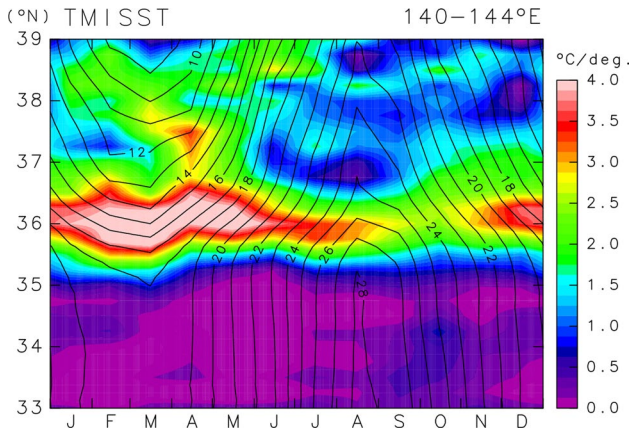

Fig. 4 Seasonal cycles of monthly climatological SST (contours) and its meridional gradient (tones) averaged in 140°E to 144°E. The contour interval is 1 °C. The sign of the meridional gradient is reversed

the SST is sustained in a small region along the SST front from June to July. In addition, the SST difference depicted in Fig. 3 shows a similar pattern to the ADT difference between June and July, although the large-scale ADT difference averaged around the KE region is almost zero (not shown).

In the present study, only data for 10 years from 2001 to 2010 were analyzed because of the limitation of satellite observation. While one may concern dependency of the results on the stability of the KE, the maintenance or intensification of the SST front was statistically detected even when we selected only 5 years with an unstable state of the KE (2001, 2006, 2007, 2008, and 2009) (not shown).

Figure 4 depicts the meridional SST gradient averaged from 140°E to 144°E where the SST gradient along the KE is large in Fig. 2. In general, the gradient is gradually weakened from spring to summer. However, when we focus on the SST gradient near 36°N during early summer, a large SST gradient (>3 °C/deg.) is found to be sustained locally

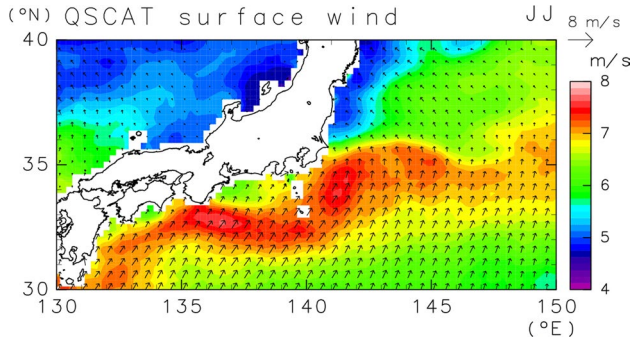

Fig. 5 Sea-surface wind vector (*arrows*) and scalar wind speed (tones) averaged for June and July from 2001 to 2009

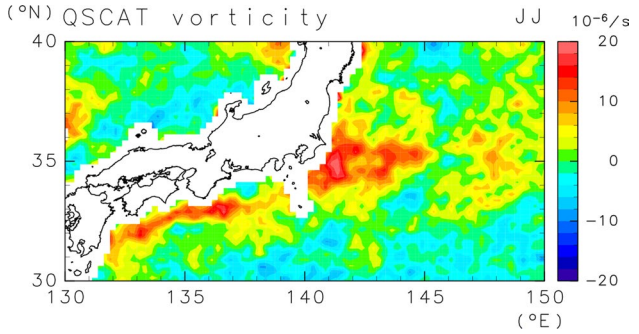

Fig. 7 Relative vorticity of sea-surface wind averaged for June and July of 2001 to 2009

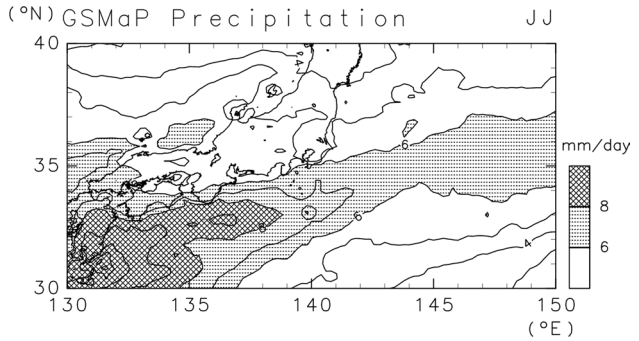

Fig. 6 Precipitation rate averaged for June and July from 1979 to 2011. The contour interval is 1 mm/day. Precipitation rates above 4 mm/day (8 mm/day) are *shaded* (*hatched*)

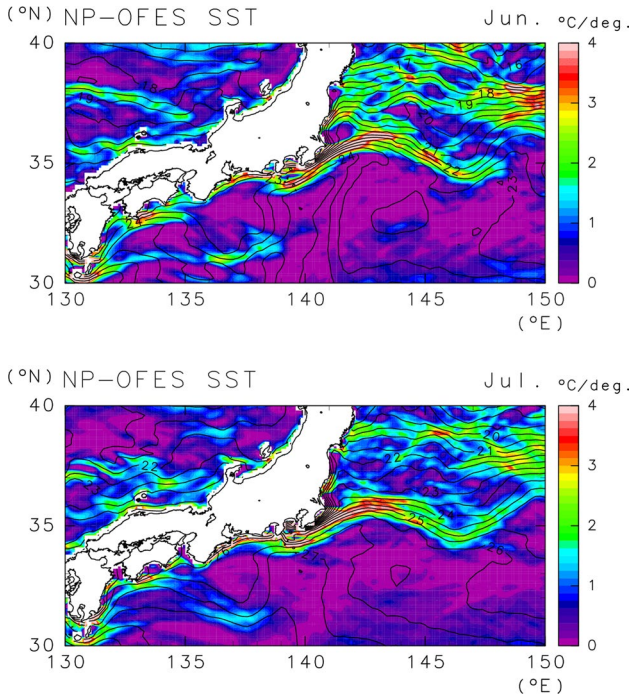

Fig. 8 Simulated SST (contours) and its meridional gradient (tones) averaged for (*top*) June and (*bottom*) July from 2001 to 2010. The contour interval is 0.5 °C

along the KE from June to July. In addition, the SST front moves slightly southward. This SST front becomes vague in late summer (after August). Therefore, the seasonal cycle of the SST around 36°N is quite asymmetric between early and late summer. No such a characteristic seasonal cycle is identified from 144°E to 148°E (not shown).

In Fig. 5, strong surface southwesterlies are identified along the Kuroshio/KE regions. Much precipitation is also observed in the same location (Fig. 6). This precipitation zone situated around 33°N to 35°N corresponds to the BFZ. In Fig. 5, the zonal component of the surface wind is positive (westerly) to the south of the current axis indicated in Figs. 1 and 2, while it is near zero or negative (easterly) on the northern side of the current. Therefore, positive vorticity is produced associated with the meridional shear of zonal wind over the KE region in June and July (Fig. 7). The positive vorticity is predominant particularly in the upstream KE region near the eastern tip of Japan (≤144°E). In general, positive vorticity in the surface wind may cause Ekman upwelling, resulting in relatively low SST (Xie et al. 2003). Such localized positive vorticity is not identified in other seasons. In winter, the sea-surface wind speed is high in this region. However, no significant horizontal wind shear associated with cumulus convection is identified since the precipitation zone is not formed in winter. In spring and autumn, the mean wind vector is nearly zero, although the sea-surface wind is strong because of transitional eddies (not shown).

3.2 Model output

First, the SSTs in June and July were compared with those of the observation. The SSTs in June and July were shown in Fig. 8. In the model, the meridional gradient

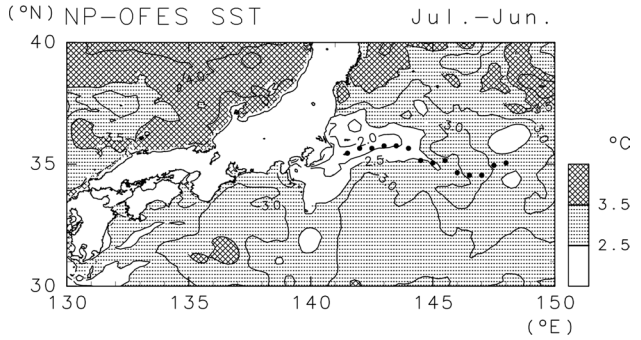

Fig. 9 Difference in simulated SSTs between June and July averaged from 2001 to 2010. The contour interval is 0.5 °C. Values above 2.5 °C (3.5 °C) are *shaded* (*hatched*). *Dots* indicate the maximum of the simulated meridional SST gradient in July

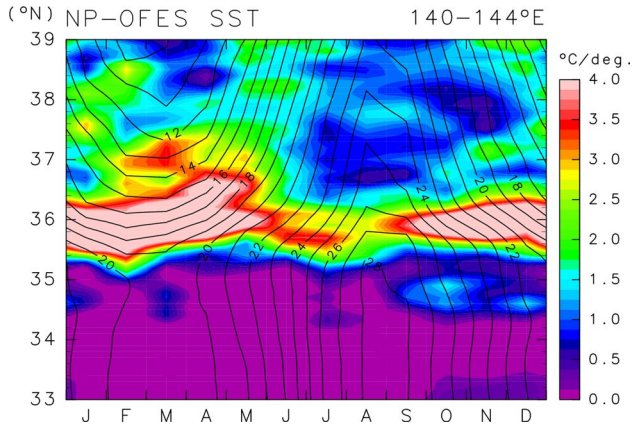

Fig. 10 Same as Fig. 4, but for the SST simulated in NP-OFES

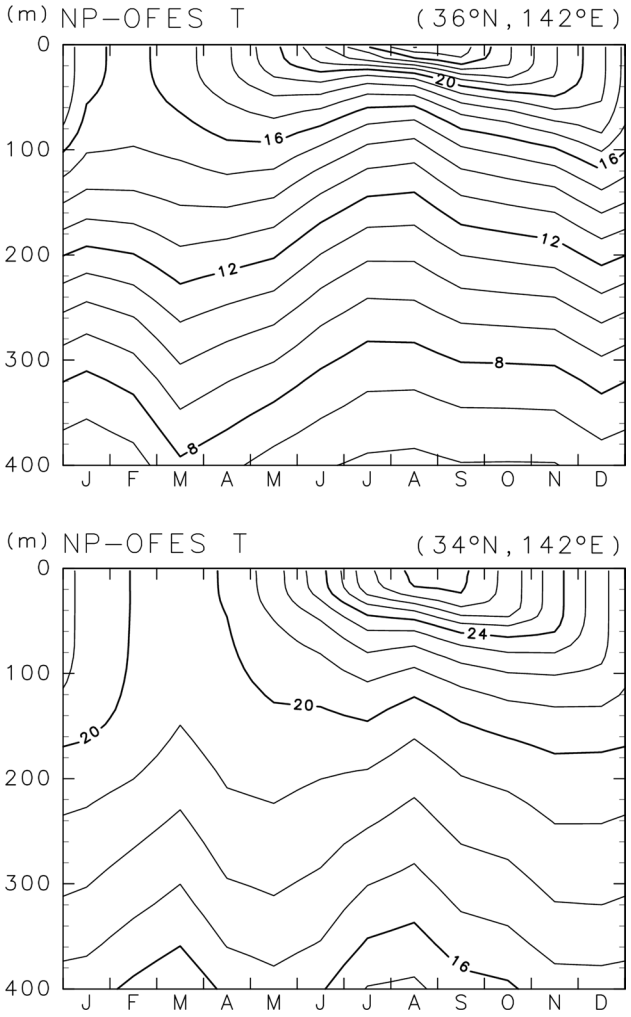

Fig. 11 Seasonal cycle of ocean temperature at (*top*) 36°N and (*bottom*) 34°N, 142°E averaged from 2001 to 2010. The contour interval is 1 °C

of the simulated SST is large at around 36°N associated with the KE, consistent with the observations (Fig. 2), although the locations of the KE and SST front are slightly shifted southward compared with the observation. Similarly to SST, the zonal current is also shifted southward (not shown). The SST difference between June and July is depicted in Fig. 9. The SST tendency is small on the northern side of the SST front, consistent with the observed result shown in Fig. 3. Moreover, the meridional gradient of the simulated SST averaged from 140°E to 144°E (Fig. 10) is also similar to the observed one (Fig. 4). On the whole, the NP-OFES appears to successfully simulate the current and SST in the KE region. Comparing Fig. 10 with Fig. 4, the seasonal march of the simulated SST front is slightly earlier than the observed one. This may be because the axis of the simulated KE and SST front is located farther south than the observation. Since the climatological BFZ and the associated surface southwesterly gradually move northward during early summer, the simulated SST front meets the BFZ earlier than the observed SST front does.

The seasonal march of ocean temperature on the northern side of the SST front is then examined. The monthly mean temperature at 36°N, 142°E is plotted in Fig. 11 (top). The mixed layer depth is about 100 m in winter. However, a shallow mixed layer forms in summer. The temperature in the mixed layer gradually increases from spring to summer. However, the ocean temperature decreases in the thermocline from June to July, associated with an upward shift of the temperature profile. Shoaling was also detected in the vertical profile of salinity (not shown). The upward motion was also clear at 34°N, 142°E on the southern side of the SST front as shown in Fig. 11 (bottom). However, the temperature decrease was less because the temperature stratification was smaller. The difference in the subsurface temperature between June and July was then analyzed in the KE region in order to clarify the vertical shift of the temperature profile and its effect on cooling of the surface layer.

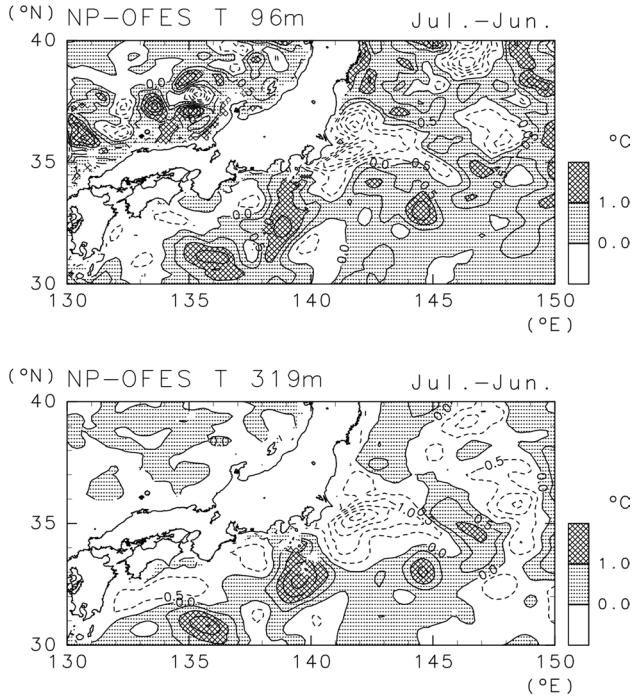

Fig. 12 Difference in simulated ocean temperatures at (*top*) 96 m and (*bottom*) 319 m between June and July (July minus June) averaged from 2001 to 2010. The contour interval is 0.5 °C. Negative contours are dotted. Values exceeding 0.0 °C (1.0 °C) are *shaded* (*hatched*)

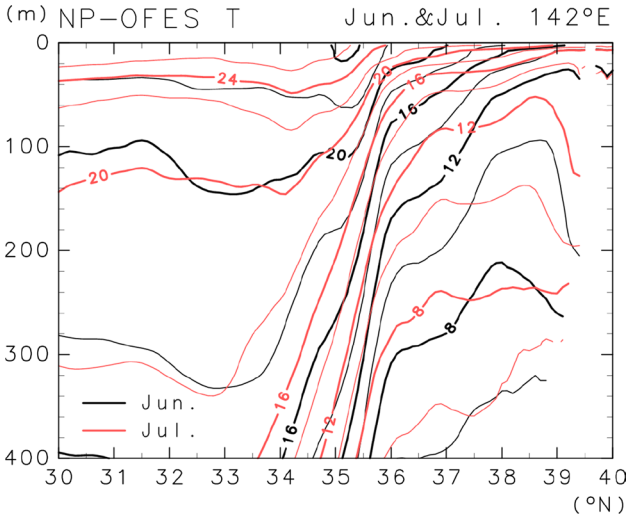

Fig. 13 Latitude-depth cross section of simulated ocean temperature along the 142°E meridian averaged for (*black*) June and (*red*) July from 2001 to 2010. The contour interval is 2 °C

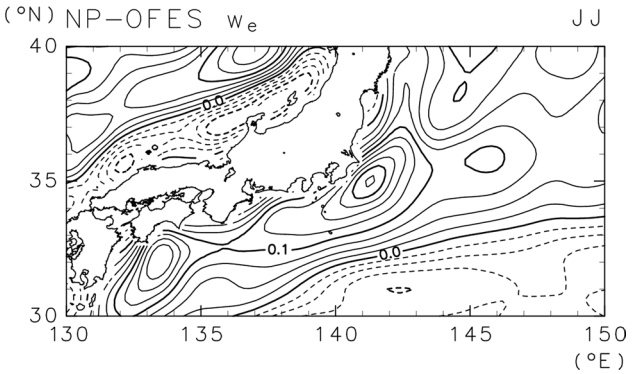

Fig. 14 Estimated Ekman upwelling averaged for June and July from 2001 to 2010. The contour interval is 0.025 m/day. Negative contours are *dotted*

Figure 12 illustrates the seasonal marches of 96 and 319 m temperatures from June to July. Since these levels correspond to the seasonal or permanent thermocline (Fig. 11), they are expected to be good indicators of the vertical shift of the temperature profile. In Fig. 12, despite being early summer, the ocean temperature decreases around the KE. Comparing the horizontal distribution of the temperature differences in Figs. 9 and 12, we find that the temperature decrease is more dominant in the subsurface than at the surface. This suggests that the dominant process related to the temperature decrease is not diabatic cooling at the surface or mechanical mixing due to surface wind. Rather, upwelling of cold subsurface water plays a significant role in the cooling. Moreover, Fig. 13 illustrates the latitude-depth cross sections of ocean temperature along 142°E in June and July. Below the 18 °C level, the temperature profile is uplifted in the region from 33°N to 37°N during early summer. The upward shift is found not only on the northern side but also on the southern side of the SST front.

The Ekman pumping velocity estimated from the wind stress that drives the model is depicted in Fig. 14. During Baiu, a strong southwesterly is centered in the southern part of the Kuroshio/KE regions as shown in Fig. 5. The zonal component of sea-surface wind is positive on the southern side of the KE, while it is nearly zero or negative on the northern side. Therefore, a large meridional shear of zonal wind is formed over the KE region. In addition, near the eastern tip of Japan (≤144°E), the southerly component of the surface wind increases with longitude. As a result, the southwesterly wind brings cyclonic vorticity over the KE region (Fig. 7), which causes the strong Ekman pumping. The positive Ekman pumping is estimated over the KE in Fig. 14. The upward shift of the isotherm depth (Fig. 13) suggests the upwelling in a large area including the Kuroshio region and the southern part of the KE region. However, the effect of Ekman pumping is confined in the western part of the KE region near Japan (≤144°E), where the small SST tendency and the subsurface temperature decrease are found (Figs. 3, 9, 12). This is in part because the stratification near the surface is larger on the northern

side associated with colder subsurface water as shown in Fig. 13. In such a region, it is inferred that the sensitivity of SST to upwelling is large.

The simulated SST front is not clear in late summer and early autumn (Fig. 10). This is similar to the observed result (Fig. 4), although the seasonal march is slightly earlier than observation. Moreover, in Fig. 11, no upwelling is simulated during this season. This is consistent with the fact that positive curl of surface wind is not identified in late summer and early autumn when the frontal zone is unclear (not shown).

4 Summary and discussion

In general, the annual range of SST is greater in high latitudes than in low latitudes. Thus, the meridional SST gradient becomes small in summer. However, on a smaller spatial scale, the meridional SST gradient across the KE is maintained or intensified during early summer. The zonal component of the sea-surface wind is high to the south of the SST front near Japan in early summer. On the other hand, the zonal wind is near zero on the northern side of the front. Therefore, the meridional shear of zonal wind contributes to positive vorticity around the SST front, resulting in Ekman upwelling in the ocean of the upstream KE region. The sensitivity of SST to upwelling is larger on the northern side of the front since the stratification is stronger. This process contributes to maintaining the SST front during Baiu.

Comparing Figs. 5 and 6, this sea-surface southwesterly coincides with a zonally elongated precipitation area observed around 33°N to 35°N associated with the BFZ. Some previous studies such as Akiyama (1973) and Pham et al. (2008) proposed that cumulus convection associated with the BFZ brings intensified westerly or southwesterly wind through vertical mixing. On the other hand, a weak easterly component on the northern side of the SST front may be associated with the cold northeasterly wind Yamase. It appears that the positive vorticity is formed by the meridional shear of zonal wind between the BFZ and the northeasterly region. In addition, in Figs. 5 and 7, the zonal shear of meridional wind also appears to contribute to the positive vorticity. More detailed analyses are required to explain the formation mechanism of such a localized wind shear over the SST front.

In Fig. 11, the thermocline is lifted up by about 20 m/month at maximum from June to July. However, the Ekman upwelling estimated in Fig. 14 is approximately 7 m/month. Thus, the simulated upwelling in Fig. 11 is larger than that predicted from Ekman upwelling. Southward shift of the KE due to some internal dynamics may cause an apparent upwelling. In addition, the area of upwelling seen in Fig. 12 is smaller than the region with cyclonic vorticity covering a wide area around the Kuroshio and KE (Fig. 14). This implies that the upward shift is localized by some internal mechanisms. First, the coastline runs from southwest to northeast in eastern Japan. Thus, the southwesterly sea-surface wind may cause coastal upwelling as well as Ekman upwelling. Moreover, the seasonality of the volume transport of Kuroshio may also affect the SST fields. According to Imawaki et al. (2001), seasonal changes in the Kuroshio transport can be estimated by satellite altimeter. From the present analyses, the meridional gradient of ADT does not decrease in early summer (not shown). Therefore, the seasonal cycle of the Kuroshio transport does not directly explain the suppression of SST warming. In any case, however, the eastward advection of the seasonal march of ocean temperature from the Kuroshio region and certain other internal dynamic processes may also be responsible for such a large upwelling. This is a subject for future studies.

These observed and simulated results suggest that the BFZ plays a specific role in maintaining or strengthening the SST front through the low-level jet. On the northern side of the BFZ, the cold northeasterly wind Yamase associated with low-level clouds may also contribute to suppressing SST warming through surface heat flux and high reflectivity. More detailed analyses may quantitatively reveal the role of low-level clouds. Conversely, the warm SST affects cumulus convection in general. Cumulus convection contributes to the formation of the low-level jet in the BFZ (Akiyama 1973). Assuming that the SST front associated with the Kuroshio/KE affects the BFZ, the BFZ may positively feed back to itself through air-sea coupling. More detailed analyses using fine-resolution atmospheric and oceanic models may clarify more precisely the mechanism of such feedback between the BFZ and Kuroshio/KE.

Acknowledgments We wish to express our gratitude to H. Nakamura at the University of Tokyo, S. Minobe of Hokkaido University, and R. Kawamura of Kyusyu University for encouragement and assistance in this work. We also thank the editor and the two anonymous reviewers for their encouragement and constructive comments. The altimeter products are produced by Ssalto/Duacs and distributed by Aviso, with support from Cnes (http://www.aviso.altimetry.fr/duacs/). TMI data are produced by Remote Sensing Systems and sponsored by the NASA Earth Science MEaSUREs DISCOVER Project. QuikScat data are produced by Remote Sensing Systems and sponsored by the National Aeronautics and Space Administration (NASA) Ocean Vector Winds Science Team. TMI and QuikScat data are available at http://www.remss.com. The GSMaP data were provided by the Japan Aerospace Exploration Agency (JAXA) (http://www.eorc.jaxa.jp/). The NP-OFES simulations were conducted on the Earth Simulator with the support of the Japan Agency for Marine-Earth Science and Technology (JAMSTEC). The GFD-DENNOU Library was utilized for drawing the figures. This study was supported by the Japan Ministry of Education, Culture, Sports, Science and Technology (MEXT) through a Grant-in-Aid for Scientific Research in Innovative Areas 2205. This work was also partly supported by the Global Environment Research Fund (2-1503) of the Ministry of the Environment, Japan.

References

Akiyama T (1973) The large-scale aspects of the characteristics of the Baiu front. Papers Meteorol Geophys 24:157–188

Alexander MA, Scott JD (2008) The role of Ekman ocean heat transport in the Northern Hemisphere response to ENSO. J Clim 21:5688–5707

Aonashi K, Liu G (2000) Passive microwave precipitation retrievals using TMI during the Baiu period of 1999. Part I: algorithm description and validation. J Appl Meteorol 39:2024–2037

Argo Science Team (2001) Argo: the global array of profiling floats. In: Koblinsky CJ, Smith NP (eds) Observing the oceans in the 21st century. GODAE Proj. Off., Melbourne, pp 248–258

CNES (2014) SSALTO/DUACS user handbook: (M)SLA and (M) ADT near-real time and delayed time products. CLS-DOS-NT-06-034 ed. 4.2, 60 p

Imawaki S, Uchida H, Ichikawa H, Fukasawa M, Umatani S, The ASUKA Group (2001) Satellite altimeter monitoring the Kuroshio transport south of Japan. Geophys Res Lett 28:17–20

Komori N, Takahashi K, Komine K, Motoi T, Zhang X, Sagawa G (2005) Description of sea-ice component of coupled Ocean-Sea-Ice Model for the Earth Simulator (OIFES). J Earth Simul 4:31–45

Kwon YO, Alexander MA, Bond NA, Frankignoul C, Nakamura H, Qiu B, Thompson LA (2010) Role of the Gulf Stream and Kuroshio-Oyashio systems in large-scale atmosphere-ocean interaction: a review. J Climate 23:3249–3281

Masumoto Y, Sasaki H, Kagimoto T, Komori N, Ishida A, Sasai Y, Miyama T, Motoi T, Mitsudera H, Takahashi K, Sakuma H, Yamagata T (2004) Fifty-year eddy-resolving simulation of the world ocean—preliminary outcomes of OFES (OGCM for the Earth Simulator). J Earth Simul 1:35–56

Minobe F, Kuwano-Yoshida A, Komori N, Xie SP, Small RJ (2008) Influence of the Gulf Stream on the troposphere. Nature 452:206–209

Nakamura H, Nishina A, Minobe S (2012) Response of storm tracks to bimodal Kuroshio path states south of Japan. J Clim 25:7772–7779

Ninomiya K (2000) Large- and meso-α-scale characteristics of Meiyu/Baiu front associated with intense rainfalls in 1–10 July 1991. J Meteorol Soc Jpn 78:141–157

Ninomiya K, Mizuno H (1985) Anomalous cold spell in summer over northeastern Japan caused by northeasterly wind from polar maritime airmass. Part 2. Structure of the northeasterly flow from polar maritime airmass. J Meteorol Soc Jpn 63:859–871

Nonaka M, Nakamura H, Tanimoto Y, Kagimoto T, Sasaki H (2006) Decadal variability in the Kuroshio-Oyashio Extension simulated in an eddy-resolving OGCM. J Clim 19:1970–1989

Nonaka M, Nakamura H, Tanimoto Y, Kagimoto T, Sasaki H (2008) Interannual-to-decadal variability in the Oyashio and its influence on temperature in the subarctic frontal zone: an eddy-resolving OGCM simulation. J Clim 21:6283–6303

Nonaka M, Sasaki H, Taguchi B, Nakamura H (2012) Potential predictability of interannual variability in the Kuroshio Extension jet speed in an eddy-resolving OGCM. J Clim 25:3645–3652

Onogi K, Tsutsui J, Koide H, Sakamoto M, Kobayashi S, Hatsushika H, Matsumoto T, Yamazaki N, Kamahori H, Takahashi K, Kadokura S, Wada K, Kato K, Oyama R, Ose T, Mannoji N, Taira R (2007) The JRA-25 Reanalysis. J Meteorol Soc Jpn 85:369–432

Pacanowski RC, Griffies SM (2000) MOM 3.0 manual. Geophysical Fluid Dynamics Laboratory/National Oceanic and Atmospheric Administration, 680 p

Pham NT, Nakamura K, Furuzawa FA, Satoh S (2008) Characteristics of low level jets over Okinawa in the Baiu and post-Baiu seasons revealed by wind profiler observations. J Meteorol Soc Jpn 86:699–717

Qiu B, Chen S, Schneider N, Taguchi B (2014) A coupled decadal prediction of the dynamic state of the Kuroshio Extension system. J Clim 27:1751–1764

Sasaki H, Klein P (2012) SSH wavenumber spectra in the North Pacific from a high-resolution realistic simulation. J Phys Oceanogr 42:1233–1241

Sasaki H, Nonaka M, Masumoto Y, Sasai Y, Uehara H, Sakuma H (2008) An eddy-resolving hindcast simulation of the quasi-global ocean from 1950 to 2003 on the earth simulator. In: Hamilton K, Ohfuchi W (eds) High resolution numerical modelling of the atmosphere and ocean. Springer, New York, pp 157–185

Sato N, Tokinaga H, Shirooka R, Suginohara N (2006) Influence of mechanical mixing on a low summertime SST in the western North Pacific ITCZ region. Geophys Res Lett 33:L14608

Taguchi B, Xie SP, Schneider N, Nonaka M, Sasaki H, Sasai Y (2007) Decadal variability of the Kuroshio Extension: observations and an eddy-resolving model hindcast. J Clim 20:2357–2377

Taguchi B, Nakamura H, Nonaka M, Xie SP (2009) Influence of the Kuroshio/Oyashio Extensions on air–sea heat exchanges and storm-track activity as revealed in regional atmospheric model simulations for the 2003/04 cold season. J Clim 22:6536–6560

Taguchi B, Qiu B, Nonaka M, Sasaki H, Xie SP, Schneider N (2010) Decadal variability of the Kuroshio Extension: mesoscale eddies and recirculations. Ocean Dyn 60:673–691

Tanimoto Y, Kanenari T, Tokinaga H, Xie SP (2011) Sea level pressure minimum along the Kuroshio and its Extension. J Clim 24:4419–4434

Wentz FJ, Smith DK (1999) A model function for the ocean-normalized radar cross section at 14 GHz derived from NSCAT observations. J Geophys Res 104:11499–11514

Wentz FJ, Gentemann C, Smith D, Chelton D (2000) Satellite measurements of sea surface temperature through clouds. Science 288:847–850

Xie SP, Xie Q, Wang DX, Liu WT (2003) Summer upwelling in the South China Sea and its role in regional climate variations. J Geophys Res 108:3261. doi:10.1029/2003JC001867

Xue H, Bane JM Jr, Goodman LM (1995) Modification of the Gulf Stream through strong air–sea interactions in winter: observations and numerical simulations. J Phys Oceanogr 25:533–557

Yoshimura M (1967) Annual changes in the frontal zones in the Northern Hemisphere. Geogr Rev Jpn 40:393–408